

Carrier relaxation in GaAs v-groove quantum wires and the effects of localizationN. I. Cade,* R. Roshan, M. Hauert, A. C. Maciel, and J. F. Ryan
*Clarendon Laboratory, University of Oxford, Oxford, OX1 3PU, United Kingdom*A. Schwarz, Th. Schäpers, and H. Lüth
Institut für Schichten und Grenzflächen, Forschungszentrum, 52425 Jülich, Germany

(Received 17 June 2004; published 8 November 2004)

Carrier relaxation processes have been investigated in GaAs/ $\text{Al}_x\text{Ga}_{1-x}\text{As}$ v-groove quantum wires (QWRs) with a large subband separation ($\Delta E \approx 46$ meV). Signatures of inhibited carrier relaxation mechanisms are seen in temperature-dependent photoluminescence (PL) and photoluminescence-excitation measurements; we observe strong emission from the first excited state of the QWR below ~ 50 K. This is attributed to reduced intersubband relaxation via phonon scattering between localized states. Theoretical calculations and experimental results indicate that the pinch-off regions, which provide additional two-dimensional confinement for the QWR structure, have a blocking effect on relaxation mechanisms for certain structures within the v groove. Time-resolved PL measurements show that efficient carrier relaxation from excited QWR states into the ground state occurs only at temperatures ≥ 30 K. Values for the low-temperature radiative lifetimes of the ground- and first excited-state excitons have been obtained (340 ps and 160 ps, respectively), and their corresponding localization lengths along the wire estimated.

DOI: 10.1103/PhysRevB.70.195308

PACS number(s): 78.67.Lt, 73.21.Hb, 78.47.+p

I. INTRODUCTION

In recent years there has been considerable interest in semiconductor v-groove structures, as a means of providing a high-quality quasi-one-dimensional (1D) electronic system. This has enabled the study of fundamental physical properties in confined systems, as well as the development of novel optoelectronic structures such as quantum wire lasers.¹ Strong spatial confinement and large subband separation are essential features for room-temperature devices using these structures. However, during the growth of low-dimensional structures, interfacial roughness develops due to misorientation with the substrate,² and monolayer (ML) fluctuations.³ This results in the localization of excitons at low temperatures.^{4,5} In 1D wires these width fluctuations lead to the formation of quasi-0D quantum boxes along the wire axis,⁶ the effects of which have been observed in microphotoluminescence (μPL) measurements⁷⁻⁹ and exciton radiative lifetimes.¹⁰ Localized excitons have a key role in producing population inversion for laser emission,¹ and strongly affect the transport characteristics of 1D structures.¹¹

In this report we present time-integrated and time-resolved PL measurements and PL-excitation measurements on an array of GaAs quantum wires (QWR's) with a subband separation $> k_B T_{\text{room}}$. These measurements reveal a strong temperature dependence of carrier relaxation mechanisms between higher excited states into the ground state of the quantum wires. We find evidence of a nonthermal exciton distribution at low temperature, and ascribe this to strong exciton localization. These effects are also evident in temperature-dependent measurements of excitonic lifetimes.

A. Structure

The QWR structure studied here was prepared using a semi-insulating (100) GaAs substrate patterned with an array

of $[01\bar{1}]$ -oriented $3 \mu\text{m}$ pitch v grooves; each groove was separated by a SiO_2 photolithographic mask. A nominal 3 nm GaAs quantum well (QW) was grown within undoped $\text{Al}_{0.3}\text{Ga}_{0.7}\text{As}$ barriers by low-pressure metal-organic chemical-vapor deposition (MOCVD). Polycrystalline growth occurs on the residual SiO_2 between the grooves, which prevents the formation of a planar (100) QW at the top of the side-wall quantum wells (SQW's).¹² A cross-sectional view of a similar heterostructure is shown in the transmission electron microscope (TEM) image of Fig. 1. A crescent-shaped GaAs QWR forms at the vertex of two SQW's, separated from them by a narrow constriction or pinch-off. The well thickness in these narrow regions is 1.4 nm, and the vertical thickness of the QWR is 7.6 nm, resulting in strong 2D confinement in the wire. A vertical quantum well (VQW) also forms at the center of the groove, perpendicular to the substrate, due to the higher mobility of Ga atoms in the $\text{Al}_x\text{Ga}_{1-x}\text{As}$.¹³ More detailed reports on the growth and characterization of similar grooves are given elsewhere.^{12,14,15}

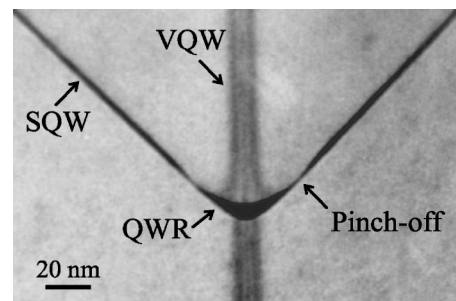


FIG. 1. TEM micrograph cross section showing the crescent-shaped QWR, which is separated from side QW's by narrow pinch-off regions. The Ga-rich VQW that also forms is seen to consist of three separate structures.

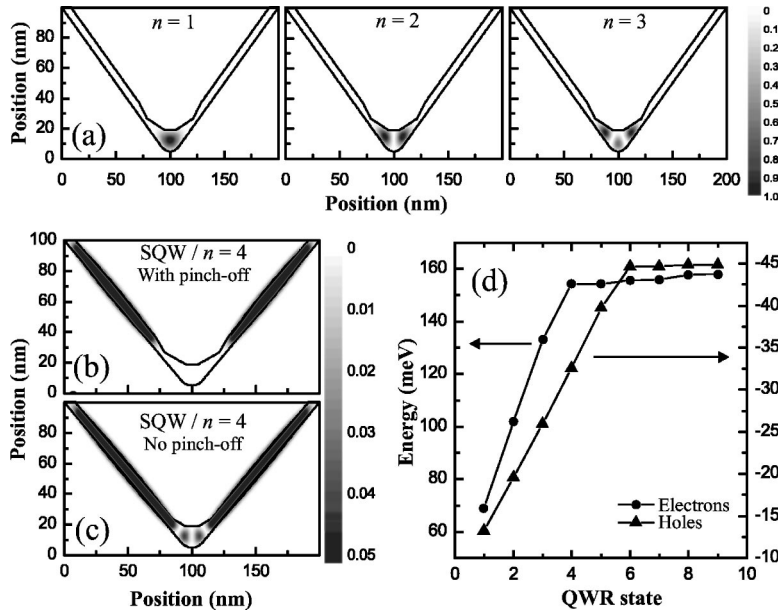


FIG. 2. (a) First three QWR electronic states (with pinch-off); (b) SQW $n=4$ state with pinch-off; (c) as (b) without pinch-off barrier included in the calculation. The shaded scales indicate the normalized relative probability density. (d) Calculated electron (circle) and heavy-hole (triangle) confinement energies for the sample under investigation.

Trapping of carriers into the QWR and the relaxation dynamics of excited states are important issues when considering carrier injection into a 1D structure. In QWR lasers carriers entering the wire region must be able to scatter into the appropriate low-energy lasing states by processes such as optical phonon emission and carrier-carrier scattering. In a v-groove structure there are two main carrier capture mechanisms: direct capture from the barrier into the QWR (3D-1D), or capture from the barrier into the SQW and VQW and then subsequent diffusion and trapping into the QWR (3D-2D-1D).^{16,17} Calculations by Kiener *et al.*¹⁸ of longitudinal-optical (LO) phonon scattering rates in a v-groove structure show that the first process is greatly reduced compared to barrier-VQW-QWR scattering, due to the small spatial overlap between initial and final states and their relatively large energy separation. Composition nonuniformity in the barrier may also significantly affect carrier capture efficiency.¹⁹ Capture into the QWR from the SQW is complicated due to the formation of the pinch-off regions and will be discussed in this report.

B. Electronic states

Electronic states of the quantum wire have been determined using a plane wave expansion to solve the Schrödinger equation for a real QWR cross section.^{20,21} These QWR profiles have been obtained directly from TEM images such as Fig. 1, and used as input data. However, in order to avoid the influences of varying image quality, the profiles shown in Fig. 2 are based on a systematic extraction of facet growth evolution.²² The size of the real-space window was limited by computational considerations, which meant that the full SQW length could not be included. The quasi-2D side-well states are therefore seen as higher-energy states of the QWR ($n \geq 4$ for electrons).

Figure 2(a) shows the electron probability density functions for the first three confined QWR states. Calculations for a 6 nm QW thickness are shown for clarity, but the results

are qualitatively the same for a 3 nm QW. All three electron states are confined within the crescent-shaped wire region, but the first two are localized on different facets. More specifically, the $n=2$ QWR state has a high probability density over the $\{311\}$ A facets that form near the bottom of the groove. These facets are expected to have quasiperiodic modulations due to step bunching,²³ with fluctuations in thickness of up to 3 ML's;²⁴ this will result in strong localization effects for excitons in the $n=2$ state.

Figures 2(b) and 2(c) show the $n=4$ state obtained with and without a pinch-off region, respectively. In the latter case the constriction is removed numerically from the QWR structural profile. This pinch-off produces an additional potential barrier between the quasi-1D and 2D states, strongly restricting $n=4$ electrons to the SQW's, with vanishing probability in the QWR itself. This results in a reduction of the overlap between QWR and SQW electronic wave functions, and hence affects the efficiency of carrier relaxation from the SQW into the QWR. Figure 2(d) shows the calculated confinement energies of the electron and heavy-hole states for the specific sample under investigation. A transition from confined QWR states to quasi-2D side-well states can be seen at $n=4$ and $n=6$ for the electron and hole states, respectively. These calculations have been performed using parabolic band approximations, whereas in reality the valence band structure is nonparabolic due to heavy- and light-hole mixing.^{25,26} The effects of the latter can be ignored if the light-hole confinement is large compared to typical heavy-hole subband separations. The heavy- and light-hole character also changes for the different subbands: calculations based on samples similar to the one considered here predict the first valence subband h_1 to be $\sim 90\%$ heavy-hole-like but h_6 is 70% light-hole-like.²⁷

II. RESULTS AND DISCUSSION

PL measurements were made using either an Ar⁺ laser operating at 2.41 eV, or a tunable dye laser (~ 1.6 – 1.8 eV),

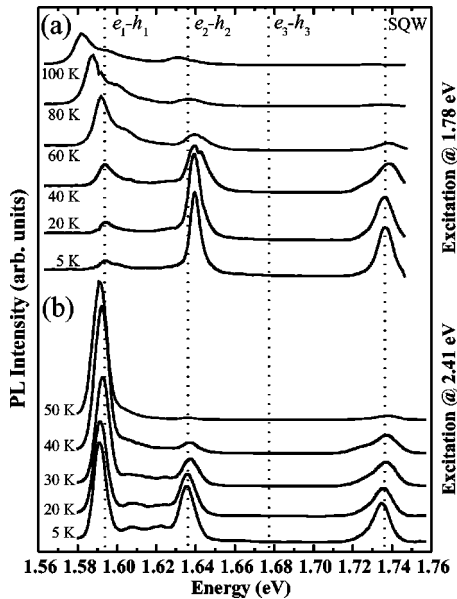


FIG. 3. Temperature-dependent PL spectra, exciting at (a) 1.78 eV and (b) 2.41 eV. The dotted lines give the theoretical energies for various QWR optical transitions.

in order to excite above or below the $\text{Al}_x\text{Ga}_{1-x}\text{As}$ band gap. The dye laser was also used for PLE measurements. Luminescence was detected with a double monochromator and either a Peltier cooled photomultiplier tube (PMT) or nitrogen-cooled charge-coupled device (CCD) depending on the experimental setup. Time-resolved PL measurements were performed using a mode-locked Ti:sapphire laser and a synchronous streak camera, with an overall time resolution of ~ 20 ps.

A. Photoluminescence measurements

Figure 3 shows the v-groove luminescence spectra as a function of temperature, when exciting with (a) the dye laser at 1.78 eV and (b) the Ar^+ laser at 2.41 eV. In the former case, only the QWR and SQW structures are excited, whereas with the Ar laser all structures and the $\text{Al}_x\text{Ga}_{1-x}\text{As}$ barrier are excited. The calculated optical transitions from the QWR are also shown. From now on we will write the electron-hole transition e_x-h_x as $n=x$. All of the calculated transition energies have been rigidly shifted so that the $n=1$ line corresponds to the low-temperature peak at 1.593 eV in Fig. 3(a), which is attributed to excitonic recombination from the $n=1$ state. The peak at 1.639 eV corresponds closely to the calculated value for recombination from the $n=2$ state. These assignments have been confirmed by magneto-PL measurements²⁸ and scanning near-field optical microscopy¹⁵ (SNOM).

The linewidths δE_{PL} of the $n=1$ and $n=2$ QWR peaks are approximately 6 meV and 7 meV, respectively, at 5 K; SNOM measurements on individual wires indicate that this broadening is due to intrawire inhomogeneities. The energy separation between the first two subband transitions ΔE is 46 meV; this large subband separation results from the small QW width and relatively strong pinch off, as well as

the specific MOCVD growth parameters.²⁹ The ratio $\rho_{\text{PL}} \equiv \Delta E / \delta E_{\text{PL}} \approx 7.7$, which is comparable to the best values of ρ_{PL} that have recently been achieved.^{29,30}

In both sets of measurements we find that there is a decrease in the $n=2$ luminescence intensity with increasing temperature. Simultaneously the $n=1$ intensity increases, indicating that intersubband relaxation of carriers is enhanced at higher temperatures due to scattering between localized states. This will be discussed in more detail with the results of the PLE measurements described below.

A predicted $n=3$ state at 1.675 eV does not appear in the PL spectra but is clearly evident in the PLE measurements. This indicates efficient relaxation to the $n=1$ state due to a significant wave-function overlap, as seen in Fig. 2(a). Luminescence from the side and vertical QWs is detected at 1.735 eV and 1.804 eV, respectively; in the former case, this corresponds to a well thickness of approximately 2.2 nm.

The power density for both excitation energies was 50 W cm^{-2} ; similar effects are observed down to 50 mW cm^{-2} corresponding to a photoexcited carrier density of $\sim 10^{12} \text{ cm}^{-2}$. When using the Ar laser, absorption in a large volume of the barrier and subsequent carrier diffusion into the QWR results in a much greater ($\sim 50\times$) wire carrier density than for excitation with the dye laser at 1.78 eV. For the latter case, the carrier population in the QWR is cooled efficiently by phonon emission; with Ar illumination absorption in the barrier generates a hot-phonon population that will facilitate exciton detrapping in the QWR. Direct capture from the VQW to the $n=1$ state is also possible with Ar illumination. This may explain why the ratio of the intensities of the $n=1$ and $n=2$ peaks is different for the two excitation energies: with Ar illumination the $n=2$ peak vanishes at 50 K, whereas it is still clearly observed at 100 K when exciting at 1.78 eV.

The low-temperature spectra in Fig. 3(b) show small luminescence peaks at 1.606 eV and 1.622 eV between the $n=1$ and $n=2$ peaks. Previous magneto-PL measurements on similar samples indicate that these may originate from higher valence band e_1-h_n excitonic transitions.²⁸ Parity-violating transitions are optically forbidden by selection rules for an ideal QWR,²⁶ but are allowed for an asymmetric wire potential, which is likely to be the case for real QWR's. Figure 3(a) also shows that, when exciting below the $\text{Al}_x\text{Ga}_{1-x}\text{As}$ band gap, the $n=1$ peak develops a high-energy shoulder above 40 K; the temperature dependence of this shoulder reflects the increased thermal population of the higher valence subbands. The redshift observed in all of the peaks above 40 K is due to the overall reduction of the band gap.

The temperature dependence of the SQW luminescence peak provides information on the real-space transfer dynamics of the structure. At 5 K there is strong luminescence with both excitation sources, which decreases with increasing temperature: the peak has almost disappeared by 50 K for excitation at 2.41 eV, but persists until ~ 80 K when excited at 1.78 eV.

Two types of potential barrier may exist that can inhibit relaxation between the SQW and QWR. Monolayer fluctuations in the $\{111\}$ side QW will trap excitons in potential minima and can have a detrapping time longer than the recombination time at low temperatures.⁴ With increasing tem-

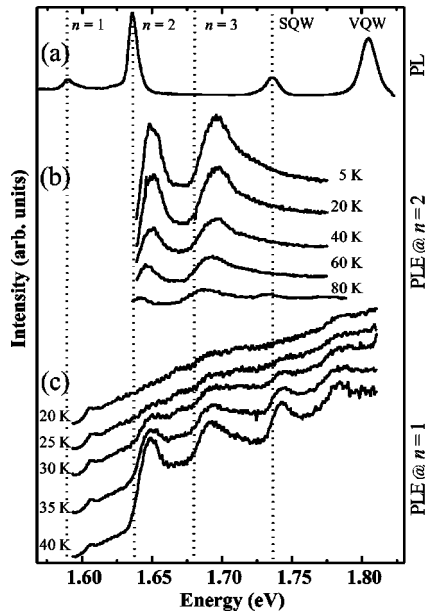


FIG. 4. (a) PL spectrum at 5 K, exciting at 1.83 eV. (b) PLE spectra as a function of temperature, detecting at the $n=2$ QWR peak energy, and (c) detecting at the $n=1$ QWR peak energy.

perature, excitons will be thermally activated and subsequently captured into the QWR. This mechanism results in a blueshift in the low-temperature SQW PL peak position with increasing temperature. As mentioned in Sec. I B, there is also a potential barrier due to the pinch-off regions, which provide 2D confinement within the quantum wire.³¹ Adiabatic calculations for this sample indicate that the pinch-off barrier is ~ 75 meV and 40 meV for electrons and heavy holes, respectively, which is consistent with the transition between confined QWR states and SQW states seen in Fig. 2(d). The spectra in Fig. 3 do show a small (~ 3 meV) blueshift in the SQW peak position over the range 5–50 K, indicating that there is some activation out of potential minima. However, the intensity of the SQW peak only starts to decrease significantly at 40 K, above which it diminishes rapidly with increasing temperature. This indicates that the pinch-off regions produce the dominant barrier for carrier transfer into the QWR.

For all of the PL peaks observed in Fig. 3, the magnitude of any thermally induced energy shift is much less than the sum of the exciton binding energy [~ 10 meV (Ref. 32)] and Stokes shift at 5 K. This indicates that emission from the QWR is dominated by excitonic recombination over the whole temperature range measured.³³

B. Photoluminescence-excitation measurements

Figure 4 shows the PL spectrum taken at 5 K and temperature-dependent PLE spectra obtained while detecting at the $n=1$ and 2 transition peaks. The PLE spectra for the $n=2$ luminescence, in Fig. 4(b), show clear absorption from the $n=2$ transition with a Stokes shift of 11 meV, as discussed below. The peak at 1.695 eV is assigned to absorption from the $n=3$ transition, which is in good agreement with the

calculated transition energy. The width of this PLE peak is greater than that of the $n=2$ peak, which is consistent with higher excited states being more sensitive to fluctuations in the confinement potential. With an increase in temperature, the intensities of both peaks decrease as fast intersubband relaxation to the ground state occurs. Above 60 K the absorption peaks shift to lower energies due to the reduction of the band-gap.

When the detection is set at the $n=1$ PL peak, in Fig. 4(c), a weak absorption peak is observed at 1.61 eV, but the spectrum is otherwise featureless below 20 K. This is consistent with the behavior of incomplete relaxation from higher energy excited states to the QWR ground state at low temperatures. The absorption at 1.61 eV is unlikely to be from the e_1-h_1 QWR transition as this would give a Stokes shift of almost 20 meV, much larger than that for the $n=2$ transition;²⁴ it is most probably from a parity-violating transition (e.g., e_1-h_2). In order to measure the $n=1$ PLE response it is necessary to set the detection to a low-energy tail state of the PL peak; however, the QWR luminescence is not strong enough to do this.

By 40 K strong features corresponding to $n=2$ and $n=3$ absorption appear in the spectra; absorption is also observed from e_1-hh_1 and e_1-lh_1 transitions in the SQW, at 1.74 eV and 1.785 eV, respectively. The transition between the regime of incomplete and efficient relaxation from higher states is clearly seen to occur over a small temperature range at ~ 30 K. The strong SQW absorption peaks appearing in the PLE also indicate efficient carrier transfer from the SQW into the QWR above 30 K, as discussed for Fig. 3. Interestingly, absorption from the SQW is not seen below 80 K when detecting at the $n=2$ energy in Fig. 4(b). This indicates that once carriers are able to transfer through the pinch-off region, they will preferentially recombine in the ground state of the QWR.

There are a number of mechanisms that can explain the inhibited inter-subband relaxation observed at low temperatures. Figure 1 shows that the VQW consists of three separate Ga-rich regions that extend upwards from different facets of the QWR. These substructures of the VQW have an Al content of $\sim 22\%$ compared to 30% in the barrier,²¹ thus generating a laterally varying potential.¹³ The first two QWR states have a real-space separation over the wire region, as shown in Fig. 2; thus the lateral potential may be sufficient to restrict relaxation from the $n=2$ QWR state at low temperature.

The sudden transition in the temperature-dependent PL and PLE spectra can also be explained by considering the role of phonons in carrier relaxation mechanisms. Generally, photo-generated electron-hole pairs will rapidly form excitons within ~ 20 ps as they simultaneously relax to the band minima:³⁴ In polar semiconductors, a hot carrier distribution can cool efficiently by emission of LO-phonons of energy $\hbar\omega_{LO}$ (36 meV for GaAs), with a characteristic time of $\sim 10^{-13}$ s. However, in 1D and 0D structures at low temperatures, the emission of high-energy LO phonons may be strongly repressed due to energy and momentum conservation,^{35,36} resulting in the controversial phonon “bottleneck” effect.³⁷ In quantum wires this is usually manifested as a reduction in intersubband relaxation.³⁸

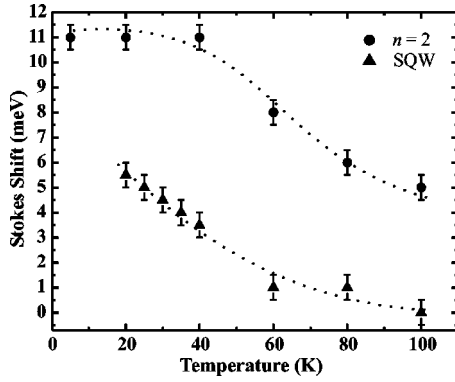


FIG. 5. Temperature dependence of the Stokes shift for the $n=2$ (circles) and SQW (triangles) transitions. The dotted lines are guides to the eye.

Longitudinal-acoustic (LA) phonons are expected to give the dominant contribution to low energy dissipation processes ($< \hbar\omega_{LO}$), but with a relatively much longer scattering time ($\sim 10^{-9}$ s). In our case, we find that the electron subband separation is comparable to $\hbar\omega_{LO}$. Even if the first-order LO-phonon coupling is forbidden, $LO \pm LA$ multiphonon processes should create a window of rapid (subnanosecond) relaxation around $\hbar\omega_{LO}$.³⁹ However, the low-temperature relaxation dynamics of photoexcited carriers are also expected to be strongly influenced by disorder. At low temperature, excitons in quasi-0D quantum dots exhibit a strong decrease in exciton-phonon scattering rates with increasing spatial quantization.⁴⁰ For strong confinement, relaxation by LA-phonon emission is much less efficient than radiative recombination, leading to very weak ground-state luminescence.

For the QWR system considered here, the $n=2$ subband is subjected to large interfacial disorder, and may be considered as a series of localized 0D states with a 1D continuum of delocalized states. By considering energy and momentum conservation arguments, the maximum acoustic phonon energy that results in significant scattering rates between quasi-0D quantum boxes is given by $E_{\max} = \hbar c_s / L_z$,⁴¹ where c_s is the sound velocity in the material (5150 ms^{-1} in GaAs) and L_z is the dimension of the strongest confinement. This latter value is 7.6 nm for our quantum wires, giving a maximum acoustic phonon energy of about 2.8 meV. Hence we would expect the peak for this phonon population to occur at a lattice temperature of ≈ 30 K. Below this temperature, exciton relaxation will be effectively inhibited due to suppression of acoustic phonon emission over the energy range of the localized states.^{6,42} Excitons will then recombine radiatively, resulting in strong luminescence at the $n=2$ level. At higher temperatures the localized excitons can relax into the ground state via phonon-assisted real-space scattering,⁴ within the exciton recombination time. This scenario is consistent with the sudden transition observed in the PLE spectra of Fig. 4(c) between 30 and 40 K.

Figure 5 shows the temperature dependence of the Stokes shift for the $n=2$ and SQW transitions, obtained from the PL and PLE spectra. In both cases the decrease of the Stokes shift with temperature reflects the thermal redistribution of excitons from localized states to extended states. For the

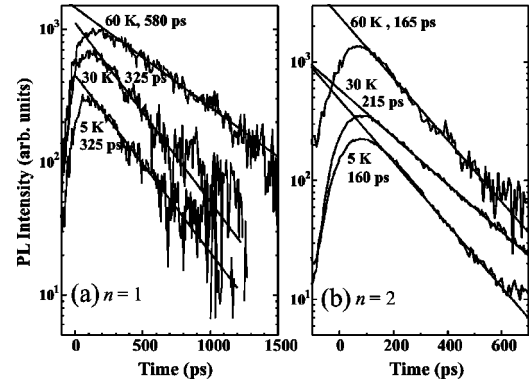


FIG. 6. Temporal profiles of the (a) $n=1$ and (b) $n=2$ luminescence peaks at three different temperatures. The monoexponential fits used to extract the decay times are shown.

SQW, the Stokes shift drops to almost zero at around 60 K, which indicates that the majority of the exciton population has become delocalized. The Stokes shift for the $n=2$ transition is relatively high at low temperatures,²⁴ and only starts to decrease around 40 K. The finite Stokes shift at 100 K indicates that there are still a significant number of $n=2$ excitons in localized states at this temperature, which is consistent with the persistence of the PL in Fig. 3.

C. Time-resolved measurements

Time-resolved PL measurements were made by exciting the sample with a mode-locked Ti:sapphire laser, operating at 76 MHz and 1.74 eV. Figures 6(a) and 6(b) show the temporal profiles of the $n=1$ and $n=2$ PL peaks, respectively, at three different lattice temperatures. All of the measured profiles show a monoexponential decay of the luminescence of the form $\exp(-t/\tau)$, over at least one order of magnitude, from which the decay time τ is obtained. By measuring the decay profiles for a range of detection energies, the temporal evolution of the PL spectra were obtained and are shown in Fig. 7 at (a) 60 K and (b) 5 K. Due to the limited set of

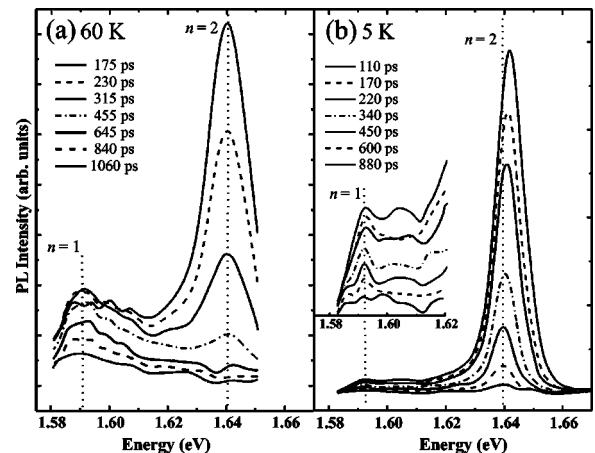


FIG. 7. Transient PL spectra (smoothed) at (a) 60 K and (b) 5 K. The inset in (b) is a magnified view of the $n=1$ peak. Note the shift in the $n=2$ peak in (b).

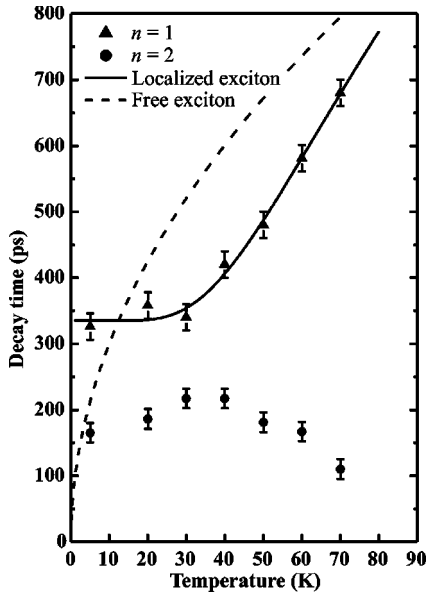


FIG. 8. Experimental luminescence decay times versus temperature, for the $n=1$ (triangles) and $n=2$ (circles) QWR states. The dashed line shows the predicted square-root dependence of the free exciton decay time with temperature, and the solid line includes localization effects, as given by Eq. (1).

detection energies sampled, it is difficult to speculate on the existence of other peaks close to the QWR ground state. At 60 K, the $n=2$ peak drops very quickly and has vanished by ~ 600 ps. However, the $n=1$ peak intensity remains essentially unchanged up to ~ 450 ps, and the emission persists at the longest measurement time. This is due to repopulation of the ground state from rapid intra- and intersubband thermalization by carrier-carrier and carrier-phonon scattering. At 5 K, the more uniform ratio of the peak intensities is indicative of frustrated intersubband relaxation and direct recombination of excited-state excitons, as discussed in the preceding section.

There are no obvious band-gap renormalization (BGR) effects as the QWR carrier density decreases with time. In the 5 K measurements, a redshift of 2.5 meV occurs in the position of the $n=2$ peak over the first 400 ps as the exciton population cools. At 60 K this transient shift is not observed, indicating that a significant number of excitons are thermally activated out of localization sites at this temperature. This is consistent with the behavior of the shifts observed in the temperature-dependent PL measurements discussed in Sec. II A, and is also consistent with the difference in Stokes shifts between 5 K and 60 K for the $n=2$ state.

The luminescence decay times of the QWR states, obtained from Fig. 6, are plotted in Fig. 8 as a function of temperature. Calculations by Citrin predict that the radiative lifetime τ_{rad} of free excitons in QWRs will follow a square-root dependence with temperature:⁴³ $\tau_{\text{rad}} \propto \sqrt{T}$. This assumes that the heterostructure is free of defects, allowing excitons to propagate freely along the wire axis. After photoexcitation, the excitons are also required to reach a thermal equilibrium on a time scale short compared to their radiative lifetime. In real heterostructures, the localization of excitons due to disorder will significantly increase their lifetime over

that of free excitons,⁴⁴ resulting in a departure from the square-root dependence at low temperatures. Figure 8 shows that the decay time of the $n=1$ state is approximately constant at low temperatures, but a rapid increase is observed above 30 K when phonon detrapping becomes effective.

Citrin's models can be modified for a 1D system of free and localized excitons in thermal equilibrium. By considering a temperature-dependent localized exciton density $N_{\text{loc}} = N_D \exp(E_{\text{loc}}/k_B T)$, Lomascolo *et al.*⁴⁵ obtain the expression given in Eq. (1) for the temperature-dependent PL decay time $\tau(T)$.

$$\tau(T) = \frac{N_D \exp(E_{\text{loc}}/k_B T) + \sqrt{\frac{2Mk_B}{\hbar^2 \pi^2}} \sqrt{T}}{\frac{N_D}{\tau_{\text{loc}}} \exp(E_{\text{loc}}/k_B T) + \frac{1}{\tau_0} \sqrt{\frac{2ME_1}{\hbar^2 \pi}}}, \quad (1)$$

where N_D is the effective density of localization centers, E_{loc} is the exciton localization energy, τ_0 and τ_{loc} are the intrinsic and localized exciton decay times, M is the total exciton mass, and E_1 is the maximum kinetic energy of radiative excitons. This method assumes that nonradiative recombination processes are negligible: we find from our measurements that the integrated intensity of the $n=1$ peak only starts to decrease at about 100 K, indicating that excitonic recombination is predominantly radiative over the temperature range considered here.

Equation (1) has been used to fit the experimental points in Fig. 8; τ_0 was fixed while N_D and E_{loc} were adjusted, and the procedure repeated to give the best fit to the data (solid line in Fig. 8). Taking $M \approx 0.3 m_0$ gives $E_1 = 0.09$ meV, and we obtain values of $N_D = 5 \times 10^4 \text{ cm}^{-1}$, $E_{\text{loc}} \approx 11$ meV, $\tau_{\text{loc}} = 340$ ps, and $\tau_0 = 130$ ps, the last being in good agreement with the predicted value.⁴³ It should be noted here that E_{loc} gives an indication of the energy required to promote localized excitons into quasi-1D continuum states *within the same subband*. Intersubband relaxation processes will be governed by a separate energy scale due to a laterally varying potential and disorder, as discussed in Sec. II B.

Calculations by Oberli *et al.*¹⁰ give the characteristic exciton localization length resulting from disorder as $l_c \propto \tau_0 / \tau_{\text{loc}}$. Based on the values obtained above, we estimate this length to be $l_c \approx 43$ nm, in agreement with Bellessa *et al.*⁷ This expression is valid for $a_B \ll l_c \ll \lambda_0/n$, where a_B and λ_0/n are the 3D exciton Bohr radius and photon wavelength in the material, respectively.

At the $n=2$ level there is a competition between relaxation into the lower subbands and recombination. The decay time for the $n=2$ state τ_2 is thus a combination of the radiative decay time $\tau_{2,\text{rad}}$ and the relaxation time $\tau_{2,\text{rel}}$, assuming again that nonradiative recombination is negligible: $\tau_2^{-1} = \tau_{2,\text{rad}}^{-1} + \tau_{2,\text{rel}}^{-1}$. Consequently, it is not straightforward to extract the two components from the measured decay times. However, the data can be interpreted qualitatively by assuming that localization effects essentially inhibit all relaxation below 30 K, and that $\tau_{2,\text{rad}} \approx \tau_2$. This is corroborated by the low-temperature PLE spectra of Fig. 4. Above 30 K, the increase in the intersubband relaxation rate is greater than the decrease in the radiative recombination rate, leading to an

overall drop in decay time. The temperature-dependent radiative efficiency $\eta(T) = \tau_2 / \tau_{2,\text{rad}}$, can be calculated from the $n=2$ peak intensities in Fig. 3. By assuming a similar behavior for $\tau_{2,\text{rad}}$ as is observed for the $n=1$ state, we obtain values of $\tau_{2,\text{rad}} = 425$ ps and $\tau_{2,\text{rel}} = 280$ ps at 60 K. Intersubband relaxation by LO-phonon emission is expected to occur on a time scale of $\sim 10^{-13}$ s for delocalized (1D) excitons; thus $\tau_{2,\text{rel}}$ gives an indication of the characteristic exciton detrapping time due to LA-phonon scattering.

In contrast to the $n=1$ state, the low-temperature radiative lifetime of the $n=2$ exciton is not much greater than the intrinsic lifetime τ_0 obtained above. The oscillator strength for a bound exciton f , and hence the radiative recombination rate, is found to scale as^{7,46}

$$f \propto \tau_{\text{rad}}^{-1} \propto V_{\text{coh}}(l_c) / V_{\text{ex}}(l_c), \quad (2)$$

where V_{coh} is the coherence volume of the exciton, which represents the spatial extent of the center-of-mass wave function of the localized exciton, and V_{ex} is the exciton volume. V_{coh} can be taken as the volume of the box in which the exciton is localized and is proportional to l_c . For $l_c > a_B$, the exciton volume is constant and a reduction of l_c leads to a reduction of the oscillator strength (i.e., an increase in the radiative lifetime above τ_0). This is observed for the $n=1$ transition and is consistent with the value of l_c obtained above ($a_B \approx 12$ nm for GaAs). If $l_c \lesssim a_B$, and the exciton binding energy is smaller than the localization energy of the carriers, the electrons and holes are separately confined (strong confinement regime),^{47,48} V_{coh} is then no longer a valid quantity. The recombination rate will be determined by V_{ex}^{-1} and will increase rapidly as l_c is reduced due to compression of the electron-hole wave function.

The binding energy and radius of the $n=2$ exciton were determined from magneto-PL measurements to be 9.6 meV and 10 nm, respectively.^{32,49} The low-temperature $n=2$ Stokes shift implies that the longitudinal (intrasubband) lo-

calization energy due to disorder is ≈ 11 meV, which is consistent with the value of E_{loc} obtained for the $n=1$ state. This suggests that if the characteristic localization length of the $n=2$ excitons is less than ~ 12 nm (a_B), then these excitons are strongly confined at low temperatures; hence the reduction in decay time (increased recombination rate) relative to the $n=1$ exciton.

III. CONCLUSION

In summary, we have studied carrier relaxation processes in an array of v-groove quantum wires. Luminescence measurements and theoretical models suggest that the pinch-off regions around the QWR have a blocking effect on real-space relaxation from the SQW's. In addition, relaxation from higher states of the QWR into the ground state is inhibited due to disorder induced localization of excitons in the {311} facet regions. These effects result in strong luminescence from the SQW and the first excited state of the QWR below ~ 50 K, even at low carrier densities. Evidence for the role of phonons in exciton relaxation has been found in PL, PLE, and decay-time measurements; a prominent change in characteristics is observed at ≥ 30 K when fast intersubband relaxation occurs via phonon-assisted scattering between localized states. The LA-phonon-assisted exciton detrapping time is estimated to be ~ 300 ps at 60 K. Values for the low-temperature radiative lifetimes of the ground- and first-excited-state excitons have been obtained (340 ps and 160 ps, respectively) and interpreted in terms of their corresponding localization lengths.

ACKNOWLEDGMENTS

The authors wish to thank D. Meertens for the TEM image. This work was supported by the EPSRC (U.K.) and the EC through the ULTRAFast network.

*Current address: NTT Basic Research Laboratories, Atsugi, 243-0198 Japan. Electronic address: ncade@will.brl.ntt.co.jp

¹L. Sirigu, D. Y. Oberli, L. Degiorgi, A. Rudra, and E. Kapon, Phys. Rev. B **61**, R10 575 (2000).

²F. Reinhardt, B. Dwir, G. Biasiol, and E. Kapon, J. Cryst. Growth **170**, 689 (1997).

³F. Lelarge, T. Otterburg, D. Y. Oberli, A. Rudra, and E. Kapon, J. Cryst. Growth **221**, 551 (2000).

⁴G. Bastard, C. Delalande, M. H. Meynadier, P. M. Frijlink, and M. Voos, Phys. Rev. B **29**, 7042 (1984).

⁵D. Liu and S. Das Sarma, Phys. Rev. B **51**, 13 821 (1995).

⁶J. Hasen, L. N. Pfeiffer, A. Pinezuk, S. He, K. W. West, and B. S. Dennis, Nature (London) **390**, 54 (1997).

⁷J. Bellessa, V. Voliotis, R. Grousson, X. L. Wang, M. Ogura, and H. Matsuhata, Appl. Phys. Lett. **71**, 2481 (1997); Phys. Rev. B **58**, 9933 (1998).

⁸W. R. Tribe, M. J. Steer, A. N. Forshaw, K. L. Schumacher, D. J. Mowbray, D. M. Whittaker, M. S. Skolnick, J. S. Roberts, and

G. Hill, Appl. Phys. Lett. **73**, 3420 (1998).

⁹F. Vouilloz, D. Y. Oberli, S. Wiesendanger, B. Dwir, R. Reinhardt, and E. Kapon, Phys. Status Solidi A **164**, 259 (1997).

¹⁰D. Y. Oberli, M. A. Dupertuis, F. Reinhardt, and E. Kapon, Phys. Rev. B **59**, 2910 (1999).

¹¹N. I. Cade, M. Hajipanayi, R. Roshan, A. C. Maciel, J. F. Ryan, F. Macherey, Th. Schäpers, and H. Lüth, Nanotechnology (to be published).

¹²Th. Schäpers, A. Hartmann, A. Schwarz, H. Hardtdegen, M. Bongartz, Ch. Dieker, and H. Lüth, Appl. Surf. Sci. **123/24**, 687 (1998).

¹³G. Biasiol, F. Reinhardt, A. Gustafsson, E. Martinet, and E. Kapon, Appl. Phys. Lett. **69**, 2710 (1996).

¹⁴N. I. Cade, R. Roshan, J. F. Ryan, A. C. Maciel, A. Schwarz, Th. Schäpers, and H. Lüth, Physica B **314**, 413 (2002).

¹⁵M. Hauert, R. Roshan, A. C. Maciel, J. Kim, J. F. Ryan, A. Schwarz, A. Kaluza, Th. Schäpers, and H. Lüth, in *Proceedings of the 25th International Conference on the Physics of Semicon-*

- ductors, Osaka, 2000*, edited by N. Miura and T. Ando (Springer, Berlin, 2001), p. 703.
- ¹⁶M. Walther, E. Kapon, J. Christen, D. M. Hwang, and R. Bhat, *Appl. Phys. Lett.* **60**, 521 (1992).
- ¹⁷S. C. Kan, D. Vassilovski, T. C. Wu, and K. Y. Lau, *Appl. Phys. Lett.* **62**, 2307 (1993).
- ¹⁸C. Kiener, L. Rota, A. C. Maciel, J. M. Freyland, and J. F. Ryan, *Appl. Phys. Lett.* **68**, 2061 (1996).
- ¹⁹X. L. Wang, M. Ogura, and H. Matsuhata, *Appl. Phys. Lett.* **67**, 804 (1995).
- ²⁰E. O'Sullivan, Ph.D. thesis, University of Oxford, 2000.
- ²¹A. Schwarz, Ph.D. thesis, Aachen University of Technology, 2001.
- ²²G. Biasiol, F. Lelarge, K. Leifer, and E. Kapon, *J. Cryst. Growth* **195**, 596 (1998).
- ²³G. Biasiol, F. Reinhardt, A. Gustafsson, and E. Kapon, *Appl. Phys. Lett.* **71**, 1831 (1997).
- ²⁴X. L. Wang, M. Ogura, H. Matsuhata, and A. Hamoudi, *Appl. Phys. Lett.* **71**, 2130 (1997).
- ²⁵P. C. Sercel and K. J. Vahala, *Appl. Phys. Lett.* **57**, 545 (1990).
- ²⁶U. Bockelmann and G. Bastard, *Europhys. Lett.* **15**, 215 (1991); *Phys. Rev. B* **45**, 1688 (1992).
- ²⁷F. Vouilloz, D. Y. Oberli, M.-A. Dupertuis, A. Gustafsson, F. Reinhardt, and E. Kapon, *Phys. Rev. B* **57**, 12 378 (1998).
- ²⁸A. C. Maciel, J. Kim, H. D. M. Davies, E. D. O'Sullivan, J. F. Ryan, A. Schwarz, A. Kaluza, H. Hardtdegen, Th. Schäpers, D. Meertens, Ch. Dieker, and H. Lüth, *Physica E (Amsterdam)* **6**, 530 (2000).
- ²⁹T. Otterburg, F. Lelarge, A. Rudra, and E. Kapon, *Appl. Phys. Lett.* **81**, 274 (2002).
- ³⁰X. L. Wang and M. Ogura, *J. Cryst. Growth* **221**, 556 (2000).
- ³¹X. Q. Liu, A. Sasaki, N. Ohno, Z. F. Li, W. Lu, S. C. Shen, Y. Fu, M. Willander, H. H. Tan, and C. Jagadish, *J. Appl. Phys.* **90**, 5438 (2001).
- ³²Jin Kim, Ph.D. Thesis, University of Oxford, 2000.
- ³³D. Y. Oberli, F. Vouilloz, and E. Kapon, *Phys. Status Solidi A* **164**, 353 (1997).
- ³⁴T. C. Damen, J. Shah, D. Y. Oberli, D. S. Chemla, J. E. Cunningham, and J. M. Kuo, *Phys. Rev. B* **42**, 7434 (1990).
- ³⁵U. Bockelmann and G. Bastard, *Phys. Rev. B* **42**, 8947 (1990).
- ³⁶Recent calculations suggest that renormalized LO phonons with $\omega \ll \omega_{LO}$ may contribute significantly to relaxation processes in quantum wires at low temperature. See L. Zheng and S. Das Sarma, *Phys. Rev. B* **54**, 2751 (1996).
- ³⁷H. Benisty, C. M. Sotomayor-Torres, and C. Weisbuch, *Phys. Rev. B* **44**, 10 945 (1991).
- ³⁸M. Grundmann, J. Christen, M. Joschko, O. Stier, D. Bimberg, and E. Kapon, *Semicond. Sci. Technol.* **9**, 1939 (1994).
- ³⁹T. Inoshita and H. Sakaki, *Phys. Rev. B* **46**, 7260 (1992).
- ⁴⁰U. Bockelmann, *Phys. Rev. B* **48**, 17 637 (1993).
- ⁴¹H. Benisty, *Phys. Rev. B* **51**, 13 281 (1995).
- ⁴²D. Y. Oberli, F. Vouilloz, R. Ambigrahy, B. Deveaud, and E. Kapon, *Phys. Status Solidi A* **178**, 211 (2000).
- ⁴³D. S. Citrin, *Phys. Rev. Lett.* **69**, 3393 (1992).
- ⁴⁴D. S. Citrin, *Phys. Rev. B* **47**, 3832 (1992).
- ⁴⁵M. Lomascolo, P. Ciccarese, R. Cingolani, and R. Rinaldi, *J. Appl. Phys.* **83**, 302 (1998).
- ⁴⁶J. Feldmann, G. Peter, E. O. Göbel, P. Dawson, K. Moore, C. Foxon, and R. J. Elliot, *Phys. Rev. Lett.* **59**, 2337 (1987).
- ⁴⁷Y. Kayanuma, *Phys. Rev. B* **38**, 9797 (1988).
- ⁴⁸R. C. Iotti and L. C. Andreani, *Phys. Rev. B* **56**, 3922 (1997).
- ⁴⁹The exciton radius in a quantum wire is highly anisotropic and is found to be significantly smaller in the confined directions. The value given is the maximum radius in the direction of the wire. See Y. Nagamune, Y. Arakawa, S. Tsukamoto, M. Nishioka, S. Sasaki, and N. Miura, *Phys. Rev. Lett.* **69**, 2963 (1992).